Integrated model for chemically enhanced physical vapor deposition of tantalum nitride-based films

Ning Li, P. W. Brenner,[a] and D. N. Ruzic[b]
Plasma Materials Interactions Group, University of Illinois at Urbana-Champaign, Urbana, Illinois 61801

(Received 20 September 2005; accepted 1 March 2006; published 21 April 2006)

A zero-order semiempirical model has been developed for chemically enhanced physical vapor deposition (CEPVD), a recently developed hybrid approach to film deposition offering the step coverage of chemical vapor deposition while maintaining film quality similar to films produced by ionized physical vapor deposition (IPVD). CEPVD is done by introducing a chemical precursor to the substrate during IPVD. A synergistic effect between the two processes results in which the high energy ions from IPVD aid in the decomposition of the precursor. The precursor then provides film deposition on surfaces that are not easily impacted by IPVD's directional ions. The model stems from knowledge of reactive sputtering and plasma-enhanced chemical-vapor deposition processes as well as results acquired from CEPVD experiment. It focuses on the Ta–N material system since Ta/TaN is widely used as a diffusion barrier in Cu damascene processing. Processing parameters are correlated with the target and film surface coverage by Ta, TaN, and organic sites, from which one can predict the operation mode, either metallic or poison, and the film elemental composition. The organic by-products accounting for the detection of carbon on the substrate by Auger electron spectroscopy analysis and poisoning of the target during the processing are categorized into nonvolatile products (OR1) and volatile products (OR2) in a lump-sum assumption. Electron impact, H reduction and ion bombardment are considered as the enhancing mechanisms between the physical and chemical components and included as the reactants of the chemical reactions. Simulation results compare favorably with the experimental data. © *2006 American Vacuum Society.* [DOI: 10.1116/1.2190659]

I. INTRODUCTION

The integration of copper liners in advanced metallization systems requires a thermally stable and reliable diffusion barrier. As the critical dimension scales below 0.1 μm, future barriers need to be functional at minimal occupancy in the trench or via lining. Physical vapor deposition (PVD) using ionized metal plasmas (ionized PVD or IPVD) is widely used to deposit conducting diffusion barriers and liners such as Ta and TaN for use in ultra-large-scale integrated (ULSI) interconnect stacks. Ionized PVD films exhibit low resistivity, high density, and good adhesion to the underlying dielectric desired for this application. On the other hand, extending PVD beyond the 45 nm technology node is problematic since IPVD may not provide sufficient step coverage to reliably coat features having high aspect ratio and sub-100 nm dimensions. Alternatively, chemical vapor deposition (CVD) and atomic layer deposition (ALD) can be used to deposit highly conformal metal films, but the electrical performance and surface quality may not equal that of PVD. A method providing PVD-like film quality and CVD-like step coverage is needed to address future ULSI barrier/liner deposition needs. We investigate a hybrid approach to film deposition referred to as chemically enhanced physical vapor deposition (CEPVD), in which a chemical precursor is introduced at the substrate during IPVD to provide a CVD component to the overall deposition process. In our previously reported experimental results,[1] planar CEPVD films have demonstrated a resistivity as low as 370 $\mu\Omega$ cm, close to the resistivity of an IPVD TaN film deposited in the same chamber. Compared to IPVD films deposited on high-aspect-ratio trenches [1 μm deep, aspect ratio (AR) $\sim$13], CEPVD films exhibited improved step coverage (bottom coverage $\sim$12%, side wall coverage $\sim$12%), which was comparable to the coverage of plasma-enhanced chemical-vapor deposited (PECVD) films in the same chamber.

Compared to TaN films deposited by IPVD, CEPVD "TaN" films have appreciable amounts of carbon ($\sim$30–60 at. % depending on process conditions) associated with carbide phases such as TaC and Ta_2C or with hydrocarbon incorporation.[1] The film properties demonstrate a wide range of variation with processing parameters. A physical model of plasma-precursor-surface interaction was constructed to understand the effect of all the experimental variables with the aid of Auger electron spectroscopy (AES). The model explains the film composition changes induced by the variation of the working conditions. Hydrocarbon groups which differ wildly in mass, sticking coefficient, and conductivity are expected to have a significant effect in determining CEPVD film properties.[1] Understanding the deposition physics in turn guides the further improvement of processing parameters, as discussed below. Overall, the physical model is used to hypothesize the effect of certain parameter changes on the measurable quantities, namely, the elemental compo-

[a]Electronic mail: pwbrenne@uiuc.edu
[b]Electronic mail: druzic@uiuc.edu

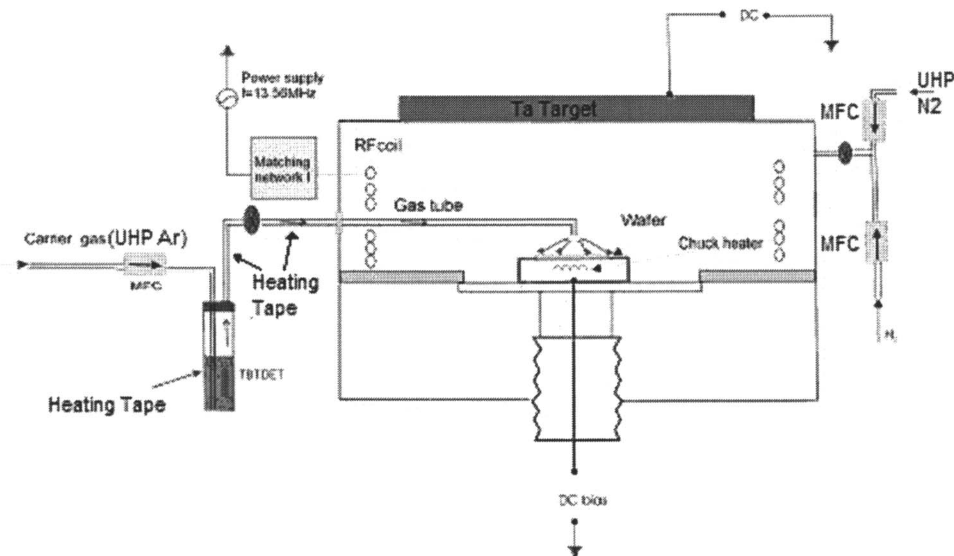

FIG. 1. Functional diagram of CEPVD experimental setup.

sition. These model predictions are verified through experimental measurements, i.e., the film stoichiometry measured by AES is compared with the results from the comprehensive model.

II. EXPERIMENTAL SETUP

The CEPVD process can be considered as a combination of CVD and PVD and so the CEPVD hardware configuration consists of both PVD and CVD components. In principle, CEPVD of tantalum nitride is carried out by introducing a Ta-containing, organometallic precursor [tert-butylimino tris-(diethylamino) tantalum, or TBTDET] in the vicinity of the substrate surface during IPVD. These experiments are conducted in a modified, commercial sputtering tool having a planar magnetron equipped with a rotating permanent magnet assembly and capable of processing 200 mm wafers (MRC Galaxy™, manufactured by Material Research Corporation, Orangeburg, NJ) (see Fig. 1). A water-cooled 35.3 cm diameter tantalum target (>99.95% purity) is used here. The apparatus and its configuration for CEPVD experiments are described in detail in Ref. 1. The process chamber is evacuated by a rotary vane roughing pump; high vacuum pumping is provided by a cryopump and a turbomolecular pump. Base pressure is 6×10^{-6} Pa (5×10^{-8} Torr). During processing, the cryopump gate valve is closed and gas flow is maintained by only the turbo pump via a throttled gate valve. Although the system is capable of coating fully 200 mm wafers, substrates in the present work are typically small coupons ($\sim3\times3$ cm^2) cleaved from a 200 mm Si wafer with 1 μm of blanket, thermal SiO_2.

Ultrahigh purity Ar is used as a buffer gas to deliver the TBTDET precursor [t-BuN=Ta(NEt_2)$_3$] vapor from the heated bubbler. Bubbler temperature is maintained at 100±5 °C. The vaporized precursor is delivered through a 3.175 mm diameter stainless steel tube that bends towards the wafer chuck to distribute the vapor over the sample coupon. Outside the vacuum chamber the tube is maintained near 100 °C to discourage condensation. The open end of the tube is 3.5 cm above the chuck. Vapor delivery sources with global uniformity suitable for large-diameter wafers (e.g., extended area shower heads) are not investigated here. H_2 is introduced to generate H radicals as the reducing agent for the chemical reactions. Chuck temperature is maintained at 350±5 °C during processing for PECVD and CEPVD experiments.

After the bubbler and wafer chuck are heated to preset temperatures, the sputtering gas (Ar), reducing agent (H_2), and reactive gas (N_2) are introduced into the chamber. Both primary and secondary plasmas are established prior to the introduction of the TBTDET vapor. N_2 functions as a reactive gas to create TaN from deposited Ta. Though this reaction could happen elsewhere, this reaction will happen primarily at the surface due to the much larger mean free path in the gas phase as compared to that at the surface. Chamber working pressure typically ranges from 11 to 16 mTorr and consists of the partial pressures of Ar, N_2, H_2, TBTDET vapor, and volatile organic by-products of the deposition process. The substrate holder is electrically isolated from ground, and ion bombardment energy is varied by application of a 0–60 V negative bias voltage to the holder. The typical working conditions are listed in Table I.

III. COMPREHENSIVE MODEL CONSTRUCTION

A zero-order semiempirical model is established for the CEPVD process. The organic compound covering the target determines the CEPVD operation mode, either metallic or poison mode. The model stems from knowledge of reactive sputtering[2–6] and PECVD processes as well as the acquired CEPVD experiment results. In turn, simulation results are used for the prediction and improvement of the CEPVD process. Improvements are made by studying the way front-end-processing parameters correlated with the chemical composition of the resultant film and the operation mode of the target.

In this model, substrate and target surfaces are subject to deposition of Ta, TaN, and hydrocarbons (OR1). The cham-

TABLE I. Typical experiment conditions and input to the simulation.

Parameter	Value
Ta sputter yield (γ_{Ta})	0.351[a]
Secondary electron yield (γ_{Se})	0.2[b]
TaN sputter yield (γ_{TaN})	0.3
Area ratio of target and substrate surface (A_t/A_s)	0.44
Effective nitrogen sticking coefficient (S_{N_2})	0.001[c]
ICP coil radius (R_c)	18 cm
ICP coil height (H_c)	7 cm
Target sputtering track ring diameter (R_t)	9 cm
Target sputtering track ring width (W_t)	7 cm
Target voltage (V_t)	400 V
Target current (I_t)	5 A
rf power (P_{abs})	410 W
Substrate bias (V_{bias})	0 V
TBTDET temperature (T_{bub})	70 °C
Substrate temperature (T_{sub})	350 °C
Chamber pressure (P_{tot})	13 mTorr
Ar flow rate (sputtering gas) ($F_{Ar\ sputter}$)	10 SCCM
Ar flow rate (carrier gas) ($F_{carrier}$)	6 SCCM
N_2 partial pressure (P_{N_2})	1.2 mTorr
H_2 flow rate (F_{H_2})	15 SCCM

[a]Reference 19.
[b]Reference 12.
[c]Reference 20.

ber is simplified into two regions, target and substrate, each involving different deposition mechanisms.[2,3] The TBTDET dispenser is mounted near the substrate and the mean free path is very short so chemical dissociation is assumed to take place only in the substrate region. The organic by-products may diffuse to the target region and stick to the target. TaN forms on the target when a nitrogen atom strikes an open Ta site. Because Ar-electron interactions are more likely to result in ionization than N-electron interactions, there will be fewer N^+ ions than Ar^+ ions. As a simplification for this model nitrogen will only be considered in molecular form and not ionized. Sputtering by the Ar ions reveals fresh Ta sites and transfers the compound from the target to the substrate. Coverage by Ta, TaN, and organic groups on both surfaces is calculated individually by balancing the surface site rate of change at steady state.

A. Chemical reactions

Generally the surface reaction mechanisms for most plasma processes are not well understood or characterized experimentally.[7] This work introduces some simple models of gas phase or surface reactions to provide some insights into the much more complicated surface processing. Though the predictions they make are useful, these models should not be regarded as completely representing the actual plasma induced reactions.

In this simplified model, chemical reactions associated with TBTDET are restricted to the substrate region, as shown in Fig. 2. The products with nonzero sticking coefficient are assumed to deposit only on the substrate surface and contribute to the surface coverage changes. Sputtering deposition also affects substrate coverage. To model this, the following procedure is used.

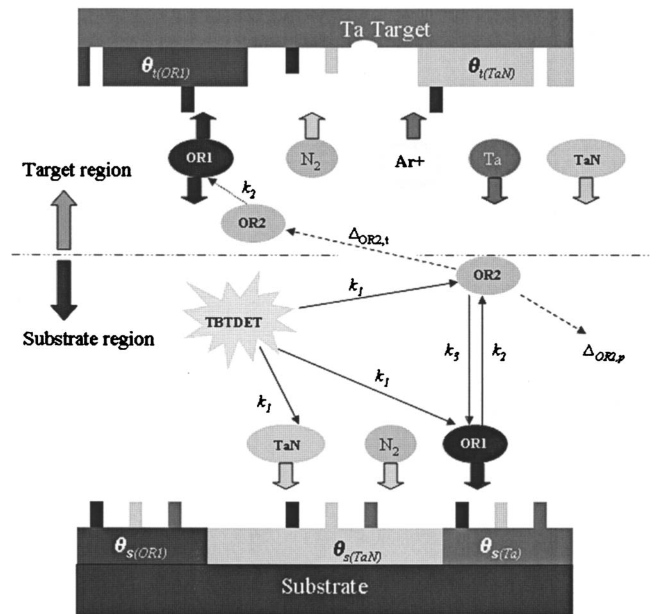

FIG. 2. Diagram of 2D CEPVD surface site dynamic model.

With the presence of plasma, TBTDET decomposition and associated interactions consist of a complex set of reactions. However, in this model, they are simplified into two pseudomolecules, nonvolatile organic product (OR1) and volatile organic product (OR2). This is a lump-sum assumption, namely, assorted volatile organic products generated in all different real-life reactions are represented as OR2 with zero sticking coefficient, while nonvolatile organic products are represented as OR1 with sticking coefficient of S_{OR1}. OR1 and OR2 both consist of C, H, and N, but with unknown stoichiometry.

In the plasma, energetic electron impact can enhance the decomposition of TBTDET in the gas phase. We represent the electron impact dissociation as reaction (1) with the third-order rate constant of $k_1^{(1)}$ (m^6/s), where $k_1^{(1)}$ is a function of electron temperature (T_e). The generated TaN and OR1 deposit on the substrate, with sticking coefficients of unity and S_{OR1}, respectively, and OR2 diffuses away from the surface boundary layer.

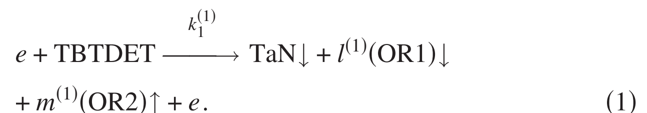

$$e + \text{TBTDET} \xrightarrow{k_1^{(1)}} \text{TaN}\downarrow + l^{(1)}(\text{OR1})\downarrow + m^{(1)}(\text{OR2})\uparrow + e. \quad (1)$$

The arrows indicate that TaN and OR1 can stick, while OR2 can only be liberated. At this point $l^{(1)}$ and $m^{(1)}$ are unknown variables.

There are other reactions for TBTDET. TBTDET can be thermally decomposed into TaN on the substrate surface at elevated temperature. This surface reaction is driven by accelerated ions through the plasma sheath. Ions inside the plasma are mostly thermalized and contribute little to the gas

phase reaction through elastic collision. It is assumed that impinging Ta ions and Ar ions accelerated by the sheath deliver the total kinetic energy to the surface energy. The enhancing mechanism is represented as reaction (2), still in the form of a gas phase reaction. Although the ions are often neutralized once they hit the surface, this process is irrelevant to any of the concerned mechanisms in this model. Thus ions still keep the charges at the right side of reaction (2). Adsorption, desorption, and diffusion surface kinetics are ignored. The rate constant associated with this surface reaction is labeled as $k_1^{(2)}$ and is dependent on substrate sheath bias voltage (V_s). The Ta ions acting as the enhancing agents come from target sputtering followed by a secondary plasma ionization process. Their occupation, of either a Ta site or a TaN site after combining with N, is counted as a result of target sputtering in a later section of this paper.

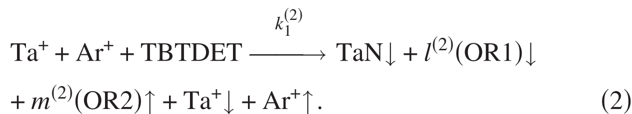

$$\mathrm{Ta}^+ + \mathrm{Ar}^+ + \mathrm{TBTDET} \xrightarrow{k_1^{(2)}} \mathrm{TaN}\downarrow + l^{(2)}(\mathrm{OR1})\downarrow + m^{(2)}(\mathrm{OR2})\uparrow + \mathrm{Ta}^+\downarrow + \mathrm{Ar}^+\uparrow. \qquad (2)$$

H radicals produced by H_2 plasma influence the gas phase decomposition reaction by reducing the activation energy of the organic precursor. In spite of the complication involved in this mechanism, the H radical enhancing mechanism is represented in reaction (3). H radicals are assumed to be incorporated into the organic products, OR1 and OR2, and therefore do not appear in the right hand side as follows:

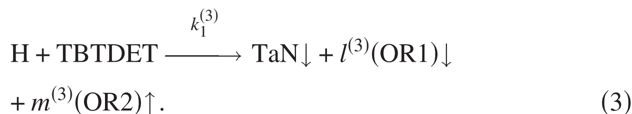

$$\mathrm{H} + \mathrm{TBTDET} \xrightarrow{k_1^{(3)}} \mathrm{TaN}\downarrow + l^{(3)}(\mathrm{OR1})\downarrow + m^{(3)}(\mathrm{OR2})\uparrow. \qquad (3)$$

Combining the three reactions, we use one pseudoreaction (4) to simulate the precursor dissociation reaction taking into account all of the enhancing mechanisms:

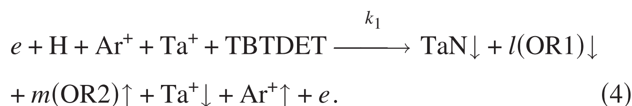

$$e + \mathrm{H} + \mathrm{Ar}^+ + \mathrm{Ta}^+ + \mathrm{TBTDET} \xrightarrow{k_1} \mathrm{TaN}\downarrow + l(\mathrm{OR1})\downarrow + m(\mathrm{OR2})\uparrow + \mathrm{Ta}^+\downarrow + \mathrm{Ar}^+\uparrow + e. \qquad (4)$$

The values l and m are determined experimentally and taken as constants in the following calculations. Note reaction (4) is in the form of a gas phase reaction but actually mixed with a surface reaction as well, where

$$k_1 \propto k_1^{(1)} + k_1^{(2)} + k_1^{(3)} = f(T_{\mathrm{sub}}, T_e, V_s). \qquad (5)$$

The function is determined empirically by means of a model with some parameters fitted by experiment data.

Define $n[\mathrm{TBTDET}]$ as the volume density of TBTDET, $n_c[\mathrm{TaN}]$ as the volume density of TaN out of chemical reaction (4), $n[\mathrm{H}]$ as the volume density of H radicals in the plasma, $n[e]$ as the electron density in the plasma, $n[\mathrm{Ta}^+]$ as the gas phase Ta ion density on the substrate surface, $n[\mathrm{Ar}^+]$ as the Ar ion density on the substrate surface, and $dn_c[\mathrm{TaN}]/dt$ as the TaN generation rate out of the chemical reaction (5).

The generation rate of TaN out of the chemical reaction is obtained from reaction (5) as follows:

$$\frac{dn_c[\mathrm{TaN}]}{dt} = k_1 n[e] n[\mathrm{TBTDET}] n[\mathrm{H}] n[\mathrm{Ta}^+] n[\mathrm{Ar}^+]. \qquad (6)$$

TaN molecules out of gas phase reactions and surface reactions deposit on the substrate surface with a sticking coefficient of 1. Notice that all the factors on the right side are time independent in a steady state plasma under the given working conditions.

The TBTDET molecule diffusion is assumed to be limited to a small region near the substrate. In this experimental configuration TBTDET molecules are only supplied through a point source that is very close to the substrate and the diffusion of such a large molecule is much slower than the other gaseous molecules. Defining the effective diffusion length as D_c, the flux of TaN molecules out of the chemical reactions is represented as

$$\Gamma_{c,\mathrm{TaN}} = D_c k_1 n[e] n[\mathrm{TBTDET}] n[\mathrm{H}] n[\mathrm{Ta}^+] n[\mathrm{Ar}^+]. \qquad (7)$$

B. Organic by-products

The organic by-products, OR1 and OR2, undergo a series of chemical reactions resulting in defragmentation and polymerization in the plasma until they are pumped away or incorporated by the surface. Given the lump-sum assumption, any products fall into the category of either OR1 or OR2 again, as reactions (8) and (9) show, where x, y, u, and v are all less than 1. The enhancing agents (electrons, H, Ta^+, or Ar^+) participating in reaction (4) can drive the conversion from OR1 to OR2, shown as follows:

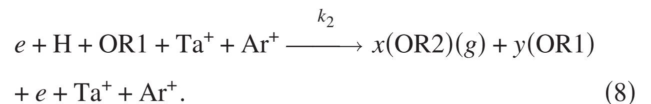

$$e + \mathrm{H} + \mathrm{OR1} + \mathrm{Ta}^+ + \mathrm{Ar}^+ \xrightarrow{k_2} x(\mathrm{OR2})(g) + y(\mathrm{OR1}) + e + \mathrm{Ta}^+ + \mathrm{Ar}^+. \qquad (8)$$

Note that $x \leqslant 1$ and $y \leqslant 1$.

The opposite conversion is rarely affected by the ion bombardment to the substrate since OR2 is assumed to be only in the gas phase. Therefore

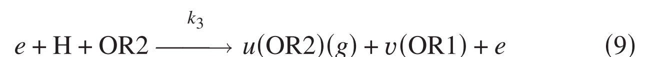

$$e + \mathrm{H} + \mathrm{OR2} \xrightarrow{k_3} u(\mathrm{OR2})(g) + v(\mathrm{OR1}) + e \qquad (9)$$

and $u \leqslant 1$ and $v \leqslant 1$.

TBTDET molecules are still thermally decomposed without the presence of the electrons, ions, and H radicals that are produced in the secondary plasma. This is represented as

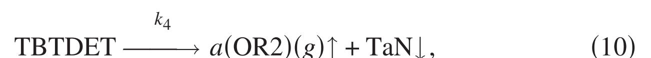

$$\mathrm{TBTDET} \xrightarrow{k_4} a(\mathrm{OR2})(g)\uparrow + \mathrm{TaN}\downarrow, \qquad (10)$$

where k_4 is only affected by the substrate temperature. The thermal decomposition organic by-product is inferred to be mostly volatiles because normally in metal-organic chemical-vapor deposition (MOCVD), the absence of the plasma causes carbon concentration in the film to be low.

Chemical reactions are not the exclusive paths for gain or loss of OR2. OR2 is removed from the chamber by the vacuum pump with a throughput of $\Delta_{\mathrm{OR2},p} n_c[\mathrm{OR2}]$, where $\Delta_{\mathrm{OR2},p}$(/s) is proportional to the pumping speed. Similarly, OR2 molecules diffuse upward from the substrate region to the target region, with a rate of $\Delta_{\mathrm{OR2},t} n_c[\mathrm{OR2}]$, and partially

convert into OR1, which getters on the target surface. OR2 concentration in the substrate is maintained constant at steady state.

Combining reactions (4), (8), and (9), we get the concentration changing rates of OR1 and OR2 which are equal to zero at steady state as follows:

$$\frac{dn_c[\mathrm{OR1}]}{dt} = lk_1 n[e]n[\mathrm{TBTDET}]n[\mathrm{H}]n[\mathrm{Ta^+}]n[\mathrm{Ar^+}] - (1-y)k_2 n[e]n[\mathrm{H}]n[\mathrm{Ta^+}]n[\mathrm{Ar^+}]n_c[\mathrm{OR1}] + vk_3 n[e]n[\mathrm{H}]n_c[\mathrm{OR2}] = 0, \quad (11)$$

$$\frac{dn_c[\mathrm{OR2}]}{dt} = mk_1 n[e]n[\mathrm{TBTDET}]n[\mathrm{H}]n[\mathrm{Ta^+}]n[\mathrm{Ar^+}] + xk_2 n[e]n[\mathrm{H}]n[\mathrm{Ta^+}]n[\mathrm{Ar^+}]n_c[\mathrm{OR1}] - (1-u)k_3 n[e]n[\mathrm{H}]n_c[\mathrm{OR2}] + ak_4 n[\mathrm{TBTDET}] - \Delta_{\mathrm{OR2},p}n_c[\mathrm{OR2}] - \Delta_{\mathrm{OR2},t}n_c[\mathrm{OR2}] = 0. \quad (12)$$

Solving Eqs. (11) and (12), we can express the OR1 and OR2 concentrations in the substrate region explicitly as follows:

$$n_c[\mathrm{OR1}] = \left\{ \frac{k_1 n[e]n[\mathrm{H}][k_3(l - lu + mv) + l(\Delta_{\mathrm{OR2},p} + \Delta_{\mathrm{OR2},t})]}{\left\{\left[\frac{1-u-(x\nu)}{(1-y)}\right]k_3 n[e]n[\mathrm{H}] + \Delta_{\mathrm{OR2},p} + \Delta_{\mathrm{OR2},t}\right\}(1-y)k_2} \right\} n[\mathrm{TBTDET}], \quad (13)$$

$$n_c[\mathrm{OR2}] = \left\{ \frac{[m + (xl)/(1-y)]k_1 n[e]n[\mathrm{H}]n[\mathrm{Ta^+}]n[\mathrm{Ar^+}] + ak_4}{\left[\frac{1-u-(x\nu)}{(1-y)}\right]k_3 n[e]n[\mathrm{H}] + \Delta_{\mathrm{OR2},p} + \Delta_{\mathrm{OR2},t}} \right\} n[\mathrm{TBTDET}]. \quad (14)$$

For a certain CEPVD system, the numerical values of k_1, k_2, k_3, k_4, l, m, u, v, x, and y are going to be determined empirically. If the physical assumptions are correct, then the film growth and characteristics can be predicted as a function of process parameters and compared to experiment. While ten unknowns appear to be an excessive number, relations for surface coverage and other plasma phenomenon reduce this number, show interrelations, and bound the possible values of the unknowns.

C. Surface coverage

The principle idea of this model is to treat the deposition surface (substrate or target surface) as a two-dimentional plane consisting of Ta, TaN, and OR1 sites. If an incident flux (Γ_j) of material j (j=Ta, TaN, or OR1) lands on a surface site of material $k \neq j$ (k= Ta, TaN, or OR1), then the coverage of j (θ_j) increases and the coverage of k (θ_k) decreases simultaneously. If the arrival flux lands on the same kind, there is no change at all due to the two-dimensional assumption. At steady state, the time changing rate of θ_j is equal to zero. It is assumed that all the sticking coefficients used in this model do not discriminate between receptor sites. The expression for substrate coverage directly correlates the chemical composition with the processing parameters.

1. Target coverage (θ_t)

Calculation of target coverage by compounds $[\theta_{t(\mathrm{TaN})}$ or $\theta_{t(\mathrm{OR1})}]$ is used to estimate the operation mode, metallic or poison, of certain working conditions. The delimitation between metallic mode or poison mode by θ_t will be determined by comparing with the experiment.

TaN coverage $[\theta_{t(\mathrm{TaN})}]$ on the target surface can be reduced by sputtering removal and overlapping by OR1 sites. Coverage can be increased by the combination of N with Ta sites. Based on the assumption that the TBTDET dissociation reaction is restricted in the substrate, the organic by-products in the target region only originate from the diffusion of the volatile molecules, namely, OR2 generated in the substrate region. The OR2 flux to the target region is then partially turned into OR1 through reactions (8) and (9) and contributes to the organic coverage $\theta_{t(\mathrm{OR1})}$ on the target. As a linear treatment, OR1 flux to the target surface is made proportional to the gas phase OR2 concentration obtained from Eq. (13) as follows:

$$\Gamma_{\mathrm{OR1},t} = c_1 n_c[\mathrm{OR2}], \quad (15)$$

where c_1 indicates the chemical reaction rate coefficients under the impact of electrons and H radicals in the primary plasma. The numerical value of c_1 is determined experimentally for the specific CEPVD system.

Define θ_t as the target compound coverage by organic group OR1 and TaN; $\theta_{t(\mathrm{OR1})}$ as the target coverage by organic group OR1; $\theta_{t(\mathrm{TaN})}$ as the target coverage by organic group TaN; γ_{Ta} as the sputter yield of the metal surface; γ_{TaN} as the sputter yield of TaN; $\gamma_{(\mathrm{OR1})}$ as the effective sputter yield of OR1, including the dissociation into volatile groups; Γi (cm^{-2} s^{-1}) as the Ar ion flux to the target; Γ_{N_2} (cm^{-2} s^{-1}) as the N_2 flux onto both target and substrate surface; $\Gamma_{\mathrm{OR1},t}$ (cm^{-2} s^{-1}) as the OR1 flux onto the target; S_{N_2} as the N_2 sticking coefficient on Ta sites; i as the number of atoms per molecule of reactive gas, here i is 2 for N_2; S_{OR1} as the OR1 sticking coefficient on Ta, TaN, and OR1 sites; $N_{t(\mathrm{TaN})}$ (cm^{-2}) as the area density of the TaN site on the target, and $N_{t(\mathrm{OR1})}$ (cm^{-2}) as the area density of the OR1 site on the target.

In reality, N_2 molecules have zero sticking coefficient on any of the sites, but N atoms can be absorbed by Ta atoms and form TaN with a reactive sticking coefficient close to 1. Therefore we relate the N_2 molecule flux to the nitride formation rate by taking the dissociation fraction of N_2 in the plasma equal to the sticking coefficient of N_2 on Ta. It is assumed that OR1 sites do not accept any nitrogen species. According to the definition of compound coverage θ_t, the Ta sites occupy the target surface in the fraction of $(1-\theta_t)$. The nitridation rate of the Ta sites on the target surface is $i\Gamma_{\mathrm{N}_2}S_{\mathrm{N}_2}(1-\theta_t)$. TaN sites are removed by Ar ion sputtering in the rate of $\Gamma_i\gamma_{\mathrm{TaN}}\theta_{t(\mathrm{TaN})}$. The OR1 flux has the sticking coefficient S_{OR1} on TaN sites as well as Ta sites. TaN sites are then replaced by the incoming OR1 flux in the rate of $\Gamma_{\mathrm{OR1},i}S_{(\mathrm{OR1})}\theta_{t(\mathrm{TaN})}$.

At steady state, the time changing rate of TaN sites on the target surface is zero. Balancing the TaN surface area density changing rate, we get

$$N_{t(\mathrm{TaN})}\frac{d\theta_{t(\mathrm{TaN})}}{dt} = i\Gamma_{\mathrm{N}_2}S_{\mathrm{N}_2}(1-\theta_t) - \Gamma_i\gamma_{\mathrm{TaN}}\theta_{t(\mathrm{TaN})} - \Gamma_{\mathrm{OR1},t}S_{(\mathrm{OR1})}\theta_{t(\mathrm{TaN})} = 0. \quad (16)$$

Similarly, the rate of OR1 formation on the target is a net result of sputtering removal [with rate $\Gamma_i\gamma_{\mathrm{OR1}}\theta_{t(\mathrm{OR1})}$] and organic flux adsorption on TaN sites and Ta sites (with rate $\Gamma_{\mathrm{OR1},t}S_{\mathrm{OR1}}[1-\theta_{t(\mathrm{OR1})}]$), which is also equal to zero at steady state as follows:

$$N_{t(\mathrm{OR1})}\frac{d\theta_{t(\mathrm{OR1})}}{dt} = \Gamma_{\mathrm{OR1},t}S_{\mathrm{OR1}}[1-\theta_{t(\mathrm{OR1})}] - \Gamma_i\gamma_{\mathrm{OR1}}\theta_{t(\mathrm{OR1})} = 0. \quad (17)$$

Target coverage of OR1 is then derived directly from Eq. (17) as follows:

$$\theta_{t(\mathrm{OR1})} = \frac{\left(\dfrac{\Gamma_{\mathrm{OR1},t}S_{\mathrm{OR1}}}{\Gamma_i\gamma_{\mathrm{OR1}}}\right)}{1+\left(\dfrac{\Gamma_{\mathrm{OR1},t}S_{\mathrm{OR1}}}{\Gamma_i\gamma_{\mathrm{OR1}}}\right)} = \frac{1}{\left(\dfrac{\Gamma_i\gamma_{\mathrm{OR1}}}{\Gamma_{\mathrm{OR1},t}S_{\mathrm{OR1}}}\right)+1}, \quad (18)$$

which mathematically shows that hydrocarbon coverage (i.e., OR1) on the target is a competing function of Ar ion sputtering and organic flux adsorption. Lower hydrocarbon contamination of the target can be achieved by increasing the Ar flow rate or target voltage. This increases Γ_i or decreases the OR1 flux by either confining the OR2 products or pumping them out.

Plugging Eq. (18) into (16) and using

$$\theta_t = \theta_{t(\mathrm{OR1})} + \theta_{t(\mathrm{TaN})} \quad (19)$$

we then solve the target coverage fraction of TaN as follows:

$$\theta_{t(\mathrm{TaN})} = \frac{1-\theta_{t(\mathrm{OR1})}}{1+(\Gamma_i\gamma_{\mathrm{TaN}}+\Gamma_{\mathrm{OR1},t}S_{\mathrm{OR1}})/i\Gamma_{\mathrm{N}_2}S_{\mathrm{N}_2}} = \frac{1/[1+(\Gamma_{\mathrm{OR1},t}S_{\mathrm{OR1}}/\Gamma_i\gamma_{\mathrm{OR1}})]}{1+(\Gamma_i\gamma_{\mathrm{TaN}}+\Gamma_{\mathrm{OR1},t}S_{\mathrm{OR1}})/i\Gamma_{\mathrm{N}_2}S_{\mathrm{N}_2}}. \quad (20)$$

The first step of Eq. (20) indicates that decreasing OR1 target coverage $\theta_{t(\mathrm{OR1})}$ exposes more Ta sites for nitride formation and thus increases TaN coverage. TaN coverage is similarly defined by the rival roles of "N_2" adsorption and sputtering removal by Ar ions.

Ta surface coverage is calculated by subtracting total compound coverage from unity as follows:

$$\theta_{t(\mathrm{Ta})} = 1-\theta_t = 1-\theta_{t(\mathrm{OR1})}-\theta_{t(\mathrm{TaN})} = \frac{1}{\{1+[i\Gamma_{\mathrm{N}_2}S_{\mathrm{N}_2}/(\Gamma_i\gamma_{\mathrm{TaN}}+\Gamma_{\mathrm{OR1},t}S_{\mathrm{OR1}})]\}[1+(\Gamma_{\mathrm{OR1},t}S_{\mathrm{OR1}}/\Gamma_i\gamma_{\mathrm{OR1}})]}. \quad (21)$$

For metallic mode operation this value should be close to 1.

2. Substrate coverage

Chemical composition of the film is derived from calculating substrate coverage of the three individual sites in this model.

Define A_t as the target area, A_s as the substrate area, θ_t as the target compound coverage by organic group OR1 and TaN, θ_s as the substrate compound coverage by organic group OR1 and TaN, $\theta_{s(\mathrm{OR1})}$ as the substrate coverage by organic group OR1, $\theta_{s(\mathrm{TaN})}$ as the substrate coverage by TaN, $N_{s(\mathrm{TaN})}$ (cm^{-2}) as the area density of the TaN site on the substrate, $N_{s(\mathrm{OR1})}$ (cm^{-2}) as the area density of the OR1 site on the substrate, and $\Gamma_{\mathrm{OR1},s}$ (cm^{-2} s^{-1}) as the OR1 flux onto

the substrate surface. Notice that

$$\theta_s = \theta_{s(\mathrm{OR1})} + \theta_{s(\mathrm{TaN})}. \tag{22}$$

Once OR1 molecules are generated from the chemical reactions (4), (8), and (9) in the substrate region, they increase the number of OR1 substrate surface sites with a rate of $\Gamma_{\mathrm{OR1},s}S_{\mathrm{OR1}}[1-\theta_{s(\mathrm{OR1})}]$. The OR1 sites on the target surface can be sputtered off and the OR1 can be redeposited on the substrate surface. The redeposition of OR1 on the substrate surface that was not covered by the OR1 sites is calculated by considering the surface area differences and the sticking coefficients. The rate equals $\Gamma_i\gamma_{(\mathrm{OR1})}\theta_{t(\mathrm{OR1})}(A_t/A_s)S_{\mathrm{OR1}}[1-\theta_{s(\mathrm{OR1})}]$. However, when Ta and TaN species are sputtered from the target and deposit on the OR1 sites, the number of OR1 sites on the substrate will decrease at the rate of $\Gamma_i\gamma_{\mathrm{Ta}}(1-\theta_t)(A_t/A_s)\theta_{s(\mathrm{OR1})}+\Gamma_i\gamma_{\mathrm{TaN}}\theta_{t(\mathrm{TaN})}(A_t/A_s)\theta_{s(\mathrm{OR1})}$. TaN flux coming from the chemical reactions (4) and (10) also covers OR1 sites and decreases the OR1 site density with the rate

$$(k_1 n[e]n[\mathrm{TBTDET}]n[\mathrm{H}]n[\mathrm{Ta}^+]n[\mathrm{Ar}^+] + k_4 n[\mathrm{TBTDET}])D_c\theta_{s(\mathrm{OR1})}.$$

At steady state, the time changing rate of substrate OR1 site coverage is equal to zero, i.e.,

$$N_{s(\mathrm{OR1})}\frac{d\theta_{s(\mathrm{OR1})}}{dt} = \Gamma_{\mathrm{OR1},s}S_{\mathrm{OR1}}[1-\theta_{s(\mathrm{OR1})}] + \Gamma_i\gamma_{(\mathrm{OR1})}\theta_{t(\mathrm{OR1})}S_{\mathrm{OR1}}\left(\frac{A_t}{A_s}\right)[1-\theta_{s(\mathrm{OR1})}] - \Gamma_i\gamma_{\mathrm{Ta}}(1-\theta_t)\left(\frac{A_t}{A_s}\right)\theta_{s(\mathrm{OR1})} - \Gamma_i\gamma_{\mathrm{TaN}}\theta_{t(\mathrm{TaN})} \times\left(\frac{A_t}{A_s}\right)\theta_{s(\mathrm{OR1})} - (k_1 n[e]n[\mathrm{TBTDET}]n[\mathrm{H}]n[\mathrm{Ta}^+]n[\mathrm{Ar}^+] + k_4 n[\mathrm{TBTDET}])D_c\theta_{s(\mathrm{OR1})} = 0. \tag{23}$$

Solving Eq. (23) for $\theta_{s(\mathrm{OR1})}$, we get

$$\theta_{s(\mathrm{OR1})} = \frac{1}{1+\left\{\dfrac{[\Gamma_i\gamma_{\mathrm{Ta}}(1-\theta_t)(A_t/A_s) + \Gamma_i\gamma_{\mathrm{TaN}}\theta_{i(\mathrm{TaN})}(A_t/A_s) + (k_1 n[e]n[\mathrm{TBTDET}]n[\mathrm{H}]n[\mathrm{Ta}^+]n[\mathrm{Ar}^+] + k_4 n[\mathrm{TBTDET}])D_c]}{[\Gamma_{\mathrm{OR1},s}S_{\mathrm{OR1}} + \Gamma_i\gamma_{(\mathrm{OR1})}\theta_{t(\mathrm{OR1})}S_{\mathrm{OR1}}(A_t/A_s)]}\right\}}, \tag{24}$$

where $(1-\theta_t)$ has been substituted in Eq. (21).

Again, TaN formation on the substrate comes both from the chemical component and physical component of ion-surface interactions (Fig. 2). First, chemical reaction (4) produces TaN flux to the substrate. TaN site coverage is increased if the flux lands on the substrate at sites that are not TaN sites. The rate of that process is $(k_1 n[e]n[\mathrm{TBTDET}]n[\mathrm{H}]n[\mathrm{Ta}^+]n[\mathrm{Ar}^+] + k_4 n[\mathrm{TBTDET}])D_c[1-\theta_{s(\mathrm{TaN})}]$. Second, TaN sputtered from the target and redepositing on the substrate also increases the TaN coverage at a rate of $\Gamma_i\gamma_{\mathrm{TaN}}\theta_{t\mathrm{TaN}}(A_t/A_s)[1-\theta_{s(\mathrm{TaN})}]$. Last, TaN site coverage increase is attributed to the nitridation of the Ta sites as well at a rate of $i\Gamma_{\mathrm{N}_2}S_{\mathrm{N}_2}(1-\theta_s)$.

The formed TaN sites can be overlapped by incident Ta from sputtering at a rate of $\Gamma_i\gamma_{\mathrm{Ta}}(1-\theta_t)(A_t/A_s)\theta_{s(\mathrm{TaN})}$. OR1, which is produced by either target sputtering or chemical reactions, covers the formed TaN sites at a rate of $\Gamma_i\gamma_{(\mathrm{OR1})}\theta_{t(\mathrm{OR1})}\times(A_t/A_s)\theta_{s(\mathrm{TaN})}S_{\mathrm{OR1}}$ and $\Gamma_{\mathrm{OR1},s}S_{\mathrm{OR1}}\theta_{s(\mathrm{TaN})}$, respectively. In steady state, the time changing rate is zero. Considering the area difference of target and substrate for the sputtering items, the TaN coverage change rate is

$$N_{s(\mathrm{TaN})}'\frac{d\theta_{s(\mathrm{TaN})}}{dt} = (k_1 n[e]n[\mathrm{TBTDET}]n[\mathrm{H}]n[\mathrm{Ta}^+]n[\mathrm{Ar}^+] + k_4 n[\mathrm{TBTDET}])D_c[1-\theta_{s(\mathrm{TaN})}] + i\Gamma_{\mathrm{N}_2}S_{\mathrm{N}_2}(1-\theta_s) + \Gamma_i\gamma_{\mathrm{TaN}}\theta_{t(\mathrm{TaN})} \times\left(\frac{A_t}{A_s}\right)(1-\theta_{s(\mathrm{TaN})}) - \Gamma_i\gamma_{\mathrm{Ta}}(1-\theta_t)\left(\frac{A_t}{A_s}\right)\theta_{s(\mathrm{TaN})} - \Gamma_i\gamma_{(\mathrm{OR1})}\theta_{t(\mathrm{OR1})}\left(\frac{A_t}{A_s}\right)\theta_{s(\mathrm{TaN})}S_{\mathrm{OR1}} - \Gamma_{\mathrm{OR1},s}S_{\mathrm{OR1}}\theta_{s(\mathrm{TaN})} = 0. \tag{25}$$

Rewriting this equation and solving for the expression of TaN coverage on the substrate gives

$$\theta_{s(\mathrm{TaN})} = \frac{1}{1 + \left\{ \frac{[i\Gamma_{\mathrm{N}_2} S_{\mathrm{N}_2} \theta_{s(\mathrm{OR1})} + \Gamma_i \gamma_{\mathrm{Ta}} (1-\theta_t)(A_t/A_s) + \Gamma_i \gamma_{(\mathrm{OR1})} \theta_{t(\mathrm{OR1})} (A_t/A_s) S_{\mathrm{OR1}} + \Gamma_{\mathrm{OR1},s} S_{\mathrm{OR1}}]}{[(k_1 n[e] n[\mathrm{TBTDET}] n[\mathrm{H}] n[\mathrm{Ta}^+] n[\mathrm{Ar}^+] + k_4 n[\mathrm{TBTDET}]) D_c + i\Gamma_{\mathrm{N}_2} S_{\mathrm{N}_2} + \Gamma_i \gamma_{\mathrm{TaN}} \theta_{t(\mathrm{TaN})} (A_t/A_s)]} \right\}}, \tag{26}$$

where $\theta_{s(\mathrm{OR1})}$ is replaced by Eq. (24).

The rest of the substrate is covered by Ta sites with a coverage of

$$\theta_{s(\mathrm{Ta})} = 1 - \theta_t = 1 - \theta_{s(\mathrm{OR1})} - \theta_{s(\mathrm{TaN})}. \tag{27}$$

D. Elemental composition of the film

Now that the expressions for the target and substrate coverage have been found, the film elemental compositions are derived from the site coverage expressions (24), (26), and (27). Note that this model assumes that the OR1 molecules consist of C and N in a certain ratio, i.e., CN_z, where z is determined empirically. It should also be noted that by chemical sputtering C can trap N in the gas phase or etch solid N off the TaN surface by chemical sputtering. Although for simplicity these reactions will not be considered here, more information are available in Refs. 8 and 9.

Ta atomic concentration is equal to the addition of TaN and Ta site coverages,

$$[\mathrm{Ta}] = [\theta_{s(\mathrm{Ta})} + \theta_{s(\mathrm{TaN})}]/[\theta_{s(\mathrm{Ta})} + 2\theta_{s(\mathrm{TaN})} + (1+z)\theta_{s(\mathrm{OR1})}]. \tag{28}$$

The TaN site coverage is taken into account in the calculation of both [Ta] and [N], so it is counted twice in the denominator of (28) in order to normalize the film composition to 1. Similarly, the OR1 site coverage is counted $(1+z)$ times in the denominator since both C and N are contained. Therefore the N atomic concentration of the film is

$$[\mathrm{N}] = [\theta_{s(\mathrm{TaN})} + z\theta_{s(\mathrm{OR1})}]/[\theta_{s(\mathrm{Ta})} + 2\theta_{s(\mathrm{TaN})} + (1+z)\theta_{s(\mathrm{OR1})}]. \tag{29}$$

Along with [Ta] and [N], this model calculates the OR1 site coverage which is proportional to the [C] in the AES analysis of the film results, i.e.,

$$[\mathrm{C}] = [\theta_{s(\mathrm{OR1})}]/[\theta_{s(\mathrm{Ta})} + 2\theta_{s(\mathrm{TaN})} + (1+z)\theta_{s(\mathrm{OR1})}]. \tag{30}$$

These expressions are calculated from the substrate and target coverages found in Sec. III C and used to compare with the experimental results from AES.

E. Integration with processing parameters

Surface coverages derived from the last section are expressed explicitly with the concentration and flux of the electrons, ions, radicals, and molecules, each of which is affected by multiple processing parameters. The model attempts to predict the variation in the film's elemental composition with the processing parameters by means of relating the explicit factors with the processing parameters. This is not trivial due to the complex chemical environment in the chamber. Other than the well-known physical relations, this work treats the undocumented ones linearly for simplification.

1. Pumping speed and diffusion rate of OR2, $\Delta_{t,\mathrm{OR2}}$, and $\Delta_{p,\mathrm{OR2}}$

The pumping speed of OR2 cannot be assessed by a simple calculation because neither the generation rate nor partial pressure of OR2 can be measured with the available experimental instruments. Therefore it must be determined empirically as shown in Sec. III F.

2. Electron temperature (T_e) and electron density ($n[e]$) of the rf plasma

Electron temperature (T_e) is the crucial factor controlling the plasma-material interactions since it governs the rate constants of the ionization of Ar and Ta and the dissociation of H_2 and N_2. Since the reaction model treats electrons, Ar^+, Ta^+, and H as reactants in the chemical reactions, T_e determines the generation rate of chemical products, TaN, OR1, and OR2, which form the coverage on both target and substrate. Calculation of electron temperature and density in the plasma is usually complicated by the electrode geometries and the cross sections of assorted collisional mechanisms. A cylindrical discharge mode is used to estimate the spatially averaged densities of the species in the model and the electron temperature in the steady state.[7,10–13] Since the electron-neutral mean free path is much shorter than the scale length of the system at the intermediate pressure region, any electron temperature and density gradients rapidly disappear through electron diffusion. It is assumed that the secondary plasma is equivalent to a near uniform cylindrical plasma of Ar and H_2 at the intermediate pressure region. The plasma perturbation induced by the volatile organic ions, metal ions, and nitrogen ions is ignored due to the relatively small concentration used in all the experiments.

3. Gas molecule density and flux, $n[\mathrm{H}]$

Gas molecule number densities of Ar, H_2, and N_2 are calculated by their partial pressures, P_{Ar}, P_{H_2}, and P_{N_2}, respectively. The gas temperature is taken as room temperature (T_g=297 K), so the neutral molecular density is calculated as

$$n_g(\mathrm{m}^{-3}) = 3.29 \times 10^{22} \times P_g(\mathrm{Torr}). \tag{31}$$

TABLE II. Regulated range of the unknown factors which restricts each term in the surface coverage expression to the range of $(0.1,10)i\Gamma_{N_2}S_{N_2}$.

Unknown factors	Likely physical bounds	Allowable range of parameter
Rate coefficient k_1	$0.1i\Gamma_{N_2}S_{N_2} \leq k_1 n[e]n[\text{TBTDET}]n[\text{H}]n[\text{Ta}^+]n[\text{Ar}^+]D_c \leq 10i\Gamma_{N_2}S_{N_2}$	6×10^{-67}–6×10^{-65}
Rate coefficient k_2	$0.1i\Gamma_{N_2}S_{N_2} \leq \Gamma_{\text{OR1},t}S_{(\text{OR1})} \leq 10i\Gamma_{N_2}S_{N_2}$	5×10^{-67}–5×10^{-65}
Rate coefficient k_3	$0.1i\Gamma_{N_2}S_{N_2} \leq \Gamma_{\text{OR1},s}S_{(\text{OR1})} \leq 10i\Gamma_{N_2}S_{N_2}$	5×10^{44}–5×10^{46}
Rate coefficient k_4	$0.01i\Gamma_{N_2}S_{N_2} \leq k_4 n[\text{TBTDET}]D_c \leq 1i\Gamma_{N_2}S_{N_2}$	15–1500
$\Delta_{t,\text{OR2},+}\Delta_{s,\text{OR2}}$	$0.1k_3 n[e]n[\text{H}] \leq \Delta_{\text{OR2},p}+\Delta_{\text{OR2},t} \leq 10k_3 n[e]n[\text{H}]$	2×10^{3}–2×10^{5}
OR1 sputter yield ($\lambda_{O_{R1}}$)	<1	0.1–0.9
OR1 sticking coefficient ($S_{O_{R1}}$)	<1	0.05–0.7
m	$m>1$	2–3
l	$t>1$	2–3
x	$0<x<1,\quad 1-u-\frac{xv}{1-y}>0$	0.2–0.4
y	$0<y<1,\quad 1-u-\frac{xv}{1-y}>0$	0.5–0.6
u	$0<u<1,\quad 1-u-\frac{xv}{1-y}>0$	0.1–0.2
v	$0<v<1,\quad 1-u-\frac{xv}{1-y}>0$	0.8–0.9
amu (OR1)	<amu (TBTDET)	Specified as 50
c_1	IF=20% AS $n[e]=2\times10^{17}/\text{m}^3$	Calculated as 1×10^{-18}
c_2	$0.1i\Gamma_{N_2}S_{N_2} \leq \Gamma_{\text{OR1},t}S_{(\text{OR1})} \leq 10i\Gamma_{N_2}S_{N_2}$	1×10^{14}–1×10^{16}
c_3	$0.1i\Gamma_{N_2}S_{N_2} \leq \Gamma_{\text{OR1},t}S_{(\text{OR1})} \leq 1i\Gamma_{N_2}S_{N_2}$	300–3000

Assume that hydrogen atoms are generated by electron impact dissociation of H_2 in the rate coefficient of $k_{\text{H,dis}}$, while lost mainly by substrate adsorption or consumption in the chemical reactions through the plasma edge. Recombination processes are small compared to the diffusion loss mechanism and are ignored. An effective plasma dimension is used instead of the actual dimension since the dissociation fraction is dependent on electron density. It is assumed that the radial and axial profiles of the hydrogen concentration are the same as those of the ion concentration, i.e., the concentration gradient only exists at the plasma sheath. At steady state, the hydrogen concentration is obtained by

$$\frac{dn[\text{H}]}{dt} = 0 = k_{\text{H,dis}} n[e] n_{g,\text{H}_2} - \frac{1}{4}\frac{n[\text{H}]\bar{v}_{\text{H}}}{d_{\text{eff}}}, \quad (32)$$

where the mean thermal velocity of hydrogen radicals following Maxwellian distribution is calculated by

$$\bar{v}_{\text{H}} = \left(\frac{8kT_g}{\pi m_{\text{H}}}\right)^{1/2}. \quad (33)$$

Two electron impact reactions are considered accounting for the generation of H radicals,[14,15]

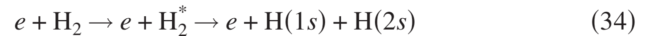

$$e + \text{H}_2 \rightarrow e + \text{H}_2^* \rightarrow e + \text{H}(1s) + \text{H}(2s) \quad (34)$$

and

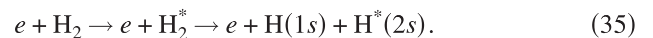

$$e + \text{H}_2 \rightarrow e + \text{H}_2^* \rightarrow e + \text{H}(1s) + \text{H}^*(2s). \quad (35)$$

The total dissociation rate constant is obtained by adding the rate constant of both reaction processes.[15] Using the reported reaction constants in Table II, we get

$$k_{\text{H,dis}}(T_e)(\text{m}^3/\text{s}) = 1.1\times10^{-15}e^{-10/T_e} + 7.89 \times 10^{-15}e^{-14.9/T_e}. \quad (36)$$

4. Sputtering Ar ion flux, Γ_i

The magnetron has a target erosion track width W_t =7 cm at R_t=9 cm. The target current I_t consists mainly of Ar ions, H ions, and ion induced secondary electrons with the emission rate of γ_{ie}. Thus total ion flux is directly related to target current by

$$\Gamma_{i,\text{tot}}(\text{cm}^2\ \text{s}) = \Gamma_{\text{Ar},t} + \Gamma_{\text{H},t} = \frac{[1/(1+\gamma_{ie})]I_t(A)}{e2\pi R_t w_t(\text{cm}^2)}. \quad (37)$$

TABLE III. List of the selected unknown factor numbers used for the simulation calculation.

Artificial factors	Selected values used for calculation
k_1	3×10^{-66}
k_2	4×10^{-66}
k_3	2×10^{-65}
k_4	50
$\Delta_{t,\mathrm{OR2}}+\Delta_{s\mathrm{OR2}}$	1×10^{5}
OR1 sputter yield (γ_{OR1})	0.65
OR1 sticking coefficient (S_{OR1})	0.1
m	2.02
l	3
x	0.4
y	0.515
u	0.1
v	0.87
c_1	1×10^{-18}
c_2	8.005×10^{14}
c_3	2×10^{3}

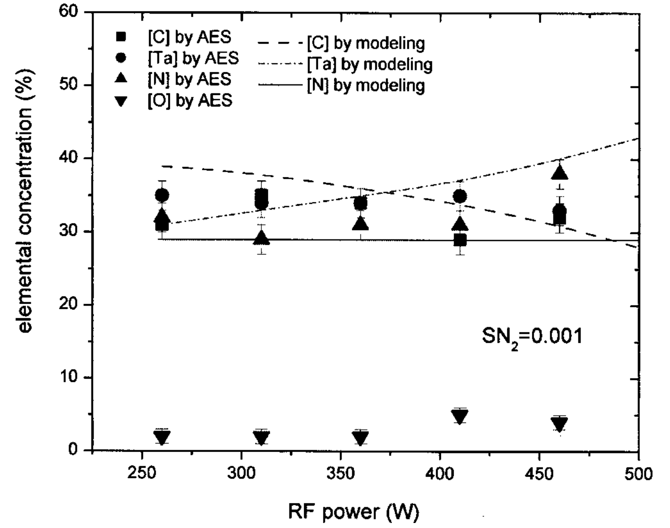

FIG. 3. Comparison of experimental results and modeling calculation of rf power effect on plasma parameters. N_2 sticking coefficient=0.001. Other working conditions are listed in Table I.

Notice that the ion velocity ($\nu_{\mathrm{Ar},t}$ and $\nu_{\mathrm{H},t}$) toward the target is accelerated by target voltage. Ar ion flux is

$$\Gamma_i = n_{i,\mathrm{Ar}} v_{\mathrm{Ar},t} = n_{i,\mathrm{Ar}}\sqrt{\frac{2eV_t}{m_{\mathrm{Ar}}}}. \tag{38}$$

H_2 ion flux is expressed by Ar ion flux as follows:

$$\Gamma_{i,\mathrm{H}} = n_{i,\mathrm{H}_2} v_{\mathrm{H}_2,t} = \alpha n_{i,\mathrm{Ar}}\sqrt{\frac{2eV_t}{m_{\mathrm{H}}}} = \alpha\sqrt{\frac{m_{\mathrm{Ar}}}{m_{\mathrm{H}}}}\Gamma_i. \tag{39}$$

Then the Ar ion flux to the target, e.g., the sputtering flux, is given by

$$\Gamma_i\,(\mathrm{m}^{-2}\,\mathrm{s}^{-1}) = \frac{\Gamma_{i,\mathrm{tot}}}{1+\alpha\sqrt{m_{\mathrm{Ar}}/m_{\mathrm{H}}}}. \tag{40}$$

The target voltage is 400 V and the current is 5 A in the experiments under typical working conditions [see Table I and H_2 flow rate of 15 SCCM (standard cubic centimeter per minute at STP)]. The model gives an Ar ion flux to the target as $5.52\times10^{19}/\mathrm{m}^2$ s. To consider reflected neutrals a SRIM simulation was performed with 400 eV Ar ions normally incident on Ta. The simulation resulted in a reflection coefficient of 0.13 and an average energy of 88.28 eV.

5. Ta ion density on the substrate, $n[\mathrm{Ta}^+]$

Let γ_{Ta} be the yield of sputtered Ta atom per incident Ar ion. The total Ta atoms enter the secondary plasma with flux

$$\Gamma_{\mathrm{Ta,tot}} = \gamma_{\mathrm{Ta}}\Gamma_i. \tag{41}$$

Ta neutrals are ionized in the plasma and accelerated to Bohm velocity by the presheath. Metal ionization fraction (IF) in an IPVD process is approximately proportional to the electron density as follows:[16,17]

$$\mathrm{IF} = c_1 n[e]. \tag{42}$$

All the other factors are synthesized into a constant c_1, which is chosen empirically in Sec. III F.

Ta ion flux to the plasma edge is accelerated by the presheath with the Bohm velocity

$$u_{B,\mathrm{Ta}} = \sqrt{\frac{kT_e}{m_{\mathrm{Ta}}}}. \tag{43}$$

Then the flux is

$$\Gamma_{\mathrm{Ta}^+} = n[\mathrm{Ta}^+]\sqrt{\frac{kT_e}{m_{\mathrm{Ta}}}}. \tag{44}$$

Surface loss of Ta ions is assumed to dominate over the volume loss. The Ta ion density at the substrate ($n[\mathrm{Ta}^+]$) is derived by balancing the increasing and decreasing rate of Ta ion species in the secondary plasma,

$$n[\mathrm{Ta}^+] = \frac{\gamma_{\mathrm{Ta}}\Gamma_i 2\pi R_t w_t \mathrm{IF}}{A_{\mathrm{eff}}\sqrt{kT_e/m_{\mathrm{Ta}}}}, \tag{45}$$

which gives the value of Ta ion density equal to $1.43\times10^{16}/\mathrm{m}^3$ under typical working conditions described above.

6. TBTDET density, n[TBTDET]

Besides the bubbler temperature and carrier gas flow rate, transportation of the TBTDET molecules from the bubbler to the chamber is affected by other factors including the viscosity of the flow, the pressure difference between the head pressure above the liquid level, and the chamber pressure and geometry of the whole delivery path. The concentration of TBTDET molecules in the substrate region is set to linearly vary with the carrier gas flow rate, F_{carrier}. Due to the small range of tuning in the bubbler temperature investigated in this project, TBTDET vapor pressure is formulated to vary

with bubbler temperature (T_{bub}) linearly. Effects from other factors on the conductance of the vapor delivery are mixed into a synthetic constant c_2, which is determined empirically for the given system,

$$n[\mathrm{TBTDET}] = c_2 T_{\mathrm{bub}} F_{\mathrm{carrier}}. \tag{46}$$

7. Nonvolatile organic product flux, $\Gamma_{OR1,t}$ and $\Gamma_{OR1,s}$

The nonvolatile organic products are prone to stick either on the substrate surface or the target surface depending on the given chamber region. The OR1 flux to the substrate is generated from the dissociation of TBTDET molecules or converted from OR2. The OR1 flux to the target is only converted from OR2 molecules that diffuse from the substrate region to the target region.

OR1 density is determined by TBTDET density, the chemical reactions, and chamber pressure, as derived in Eq. (13). The pseudo-atomic-mass units (amu) of the organic compounds (OR1 and OR2) are related based on the conservation of the molecular weights in reaction (4)

$$1 + \mathrm{amu(TBTDET)} = \mathrm{amu(TaN)} + 1 \times \mathrm{amu(OR1)} + m \times \mathrm{amu(OR2)}. \tag{47}$$

Equation (47) yields the molecular weight ratio of (OR1)/(OR2) rather than absolute values of molecular weight for OR1 and OR2. As discussed previously, the introduction of artificial constants simplifies the complicated physical and mathematical dependence while still maintaining the physical validity and the variation trend in the simulation results. With this regard, m_{OR1} is selected as 50 amu (an order of magnitude approximation) and m_{OR2} is derived from Eq. (47).

OR1 molecules in the substrate region are assumed to possess the substrate temperature T_{sub}, so the average velocity is

$$v_{\mathrm{OR1}} = \sqrt{\frac{8kT_{\mathrm{sub}}}{\pi m_{\mathrm{OR1}}}}. \tag{48}$$

Ignoring the directionality induced by the mass flow, the OR1 flux to the substrate region is obtained by

$$\Gamma_{\mathrm{OR1},s} = \tfrac{1}{4} n_c[\mathrm{OR1}] v_{\mathrm{OR1}}. \tag{49}$$

The OR1 flux to the target originates from the diffusion of the OR2 flux. Since the primary plasma parameters remain mostly unchanged we assume

$$\Gamma_{\mathrm{OR1},t} = c_3 n_c[\mathrm{OR2}], \tag{50}$$

where c_3 is taken as constant despite the complexity involved by the transport and chemistry of OR2 molecules in the plasma. c_3 is determined empirically below. OR2 concentration was derived in Eq. (14).

F. Determination of the empirical constants

Typical experimental conditions that are input into the simulation are listed in Table I unless specified in individual cases. Analyzing the surface coverage expressions, e.g.,

$$\theta_{s(\mathrm{TaN})} = \frac{1}{1 + \left\{ \dfrac{[i\Gamma_{\mathrm{N}_2} S_{\mathrm{N}_2} \theta_{s(\mathrm{OR1})} + \Gamma_i \gamma_{\mathrm{Ta}} (1-\theta_t)(A_t/A_s) + \Gamma_i \gamma_{(\mathrm{OR1})} \theta_{t(\mathrm{OR1})} (A_t/A_s) S_{\mathrm{OR1}} + \Gamma_{\mathrm{OR1},s} S_{\mathrm{OR1}}]}{[(k_1 n[e] n[\mathrm{TBTDET}] n[\mathrm{H}] n[\mathrm{Ta}^+] n[\mathrm{Ar}^+] + k_4 n[\mathrm{TBTDET}]) D_c + i\Gamma_{\mathrm{N}_2} S_{\mathrm{N}_2} + \Gamma_i \gamma_{\mathrm{TaN}} \theta_{t(\mathrm{TaN})} (A_t/A_s)]} \right\}},$$

helps determine the order of magnitude of the unknown factors that are not documented, namely, k_1, k_2, k_3, m_{OR1}, $\Delta_{t,OR2+}\Delta_{sOR2}$, c_1, c_2, and c_3. Each term in the expression represents a different mechanism that contributes to the gain or loss of the surface coverage. The values of the unknown numbers are chosen such that all terms in the coverage expression are weighted comparably or in the same order of magnitude. None of the concerned mechanisms can be ignored, since these are observed in experiment. Therefore those terms which do not contain unknown factors serve as a benchmark for the regulation process. For example, the nitridation rate of Ta sites $i\Gamma_{N_2}S_{N_2}$ contains only factors that are well documented (S_{N_2}) and straightforward to calculate (Γ_{N_2}).

Table II lists the regulated range of the artificial numbers which restrict each term in the surface coverage expression approximately to the range of $(0.1i\Gamma_{N_2}S_{N_2}, 10i\Gamma_{N_2}S_{N_2})$.

Note that the values of the rate constants k_1 seem quite unusual (i.e., 10^{-65}), but this is only an effect of scaling. They make sense since they are multiplied by five atomic densities, all in the range of $10^{16}-10^{18}$.

MATHEMATICA™ code is programed to plot with all possible combinations of the unknown factors in their allowable range as listed in Table II. The elemental composition variation versus the rf power from the experiments is compared with the simulation results in search of the proper combination of artificial factor values. The resulting combination of values that makes the simulation results best fit the experi-

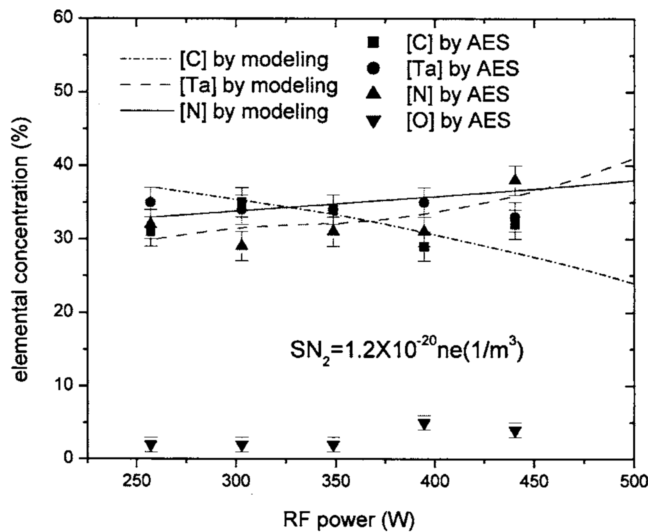

FIG. 4. Modeling of rf power effect on plasma parameters. N_2 sticking coefficient varies with electron density. Other working conditions are listed Table I.

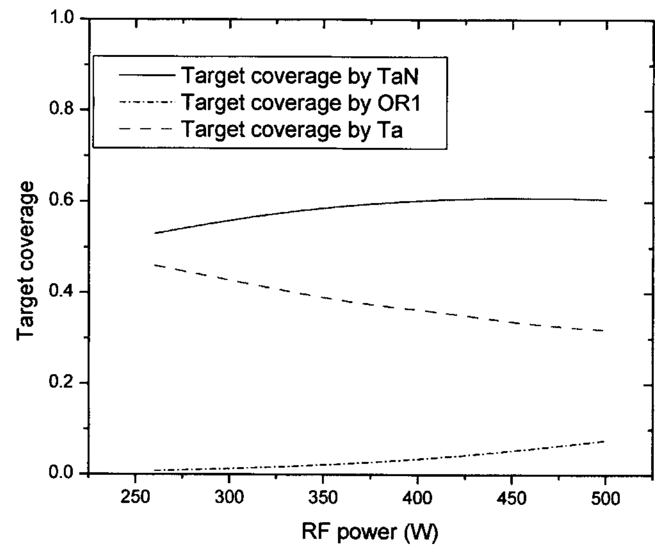

FIG. 5. Simulation result of the target coverage by Ta, OR1, and TaN sites.

mental variation trend (see Fig. 3) is listed in Table III.

The simulation result shown in Fig. 3 is not scaled; even so, it poorly reproduces the trends. Searching for other possible values did not improve the fit any further. The simulated nitrogen concentration shows little change with rf power and thus deviates from the experimental result. The model treats the electron density and ionization fraction of Ta as proportional to the rf power. As a result, the Ar ion and Ta ion densities increase significantly. The TaN site density is not changed directly because the N_2 sticking coefficient is taken as constant. Considering that the N_2 sticking coefficient is defined in the previous section as the dissociation rate of N_2 molecule density (which is approximated as proportional to the electron density), one expects a stronger dependence of nitrogen concentration on the rf power if the sticking coefficient is related to the electron density linearly. If $n[e]$ is in units of $(1/\text{m}^3)$, a better empirical relationship would be

$$SN_2 = 1.2 \times 10^{-20} n[e].$$

The constants make the sticking coefficient equal to 0.001 at an electron density of 1.2×10^{17} $(1/\text{m}^3)$, which is the typical value used in the previous discussions. The correction of the model improves the fit by increasing the [N] concentration with the rf power as shown in Fig. 4.

The modeling calculation of the target coverage (see Fig. 5) results in TaN coverage close to 60%. The target is visually found to be metallic after each experiment discussed here. The target heavily covered by an organic product looks dull and dark, and looks brownish if covered by tantalum nitride. Therefore, we specify the CEPVD process of metallic mode if the simulated TaN coverage is less than 60% for the models discussed here.

G. Comparison with other experimental results

The adopted values of those unknown factors listed in Table III are regarded as properly representing the performance of the given CEPVD system. They are fixed only by matching to the rf atomics concentration versus rf power and by using logical assertions. The next section compares simulation results with experimental results and examines the variation versus other processing parameters. Since this is a zero-order model, the simulations do not perfectly match all experimental results. The underlying physical mechanisms causing the deviation are analyzed and guide the improvement of the model. Any modifications in the model are applied to other discussions thereafter.

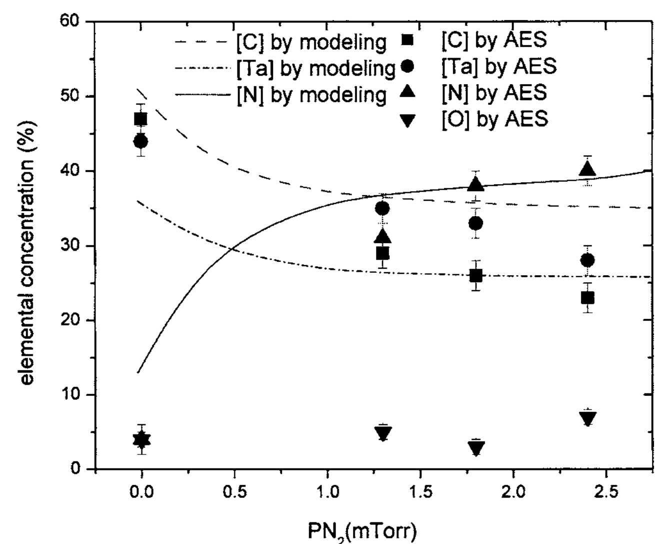

FIG. 6. Comparison of experimental results and modeling calculation of film composition variation vs N_2 partial pressure. Other working conditions are listed in Table I.

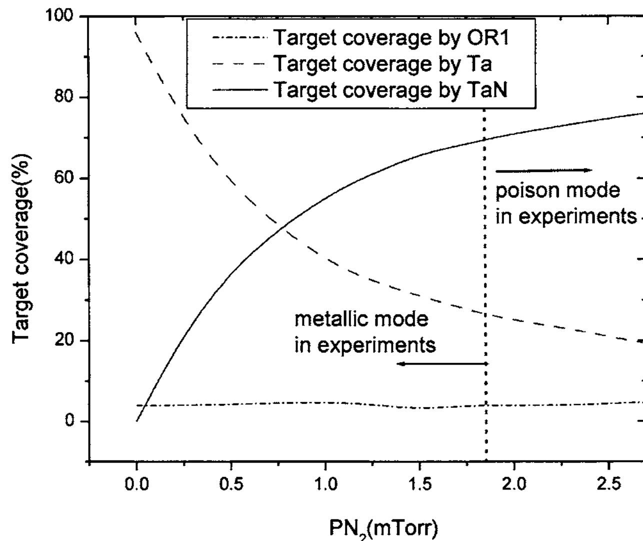

FIG. 7. Modeling results of target coverage variation vs N_2 partial pressure. The vertical dotted line marked the experiment in which the target was observed to be heavily covered by tantalum nitride.

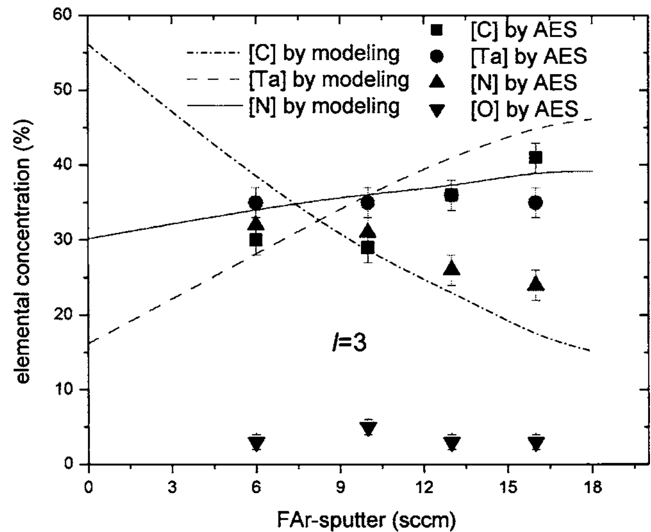

FIG. 8. Comparison of experimental results and modeling calculation of film composition variation vs Ar sputter gas flow rate. Other working conditions are listed in Table I.

1. *Effect of* N_2

Figure 6 compares the experimental and modeling results of film composition variation versus N_2 partial pressure. Nitrogen partial pressure was controlled by adjusting flow through a mass flow controller, and a quadrupole SRS RGA 100 residual gas analyzer was used to measure the partial pressure at the edge of the chamber away from the substrate. Note that the model predicts the correct trends of atomic concentration variation with N_2 partial pressure in the data. These experimental partial pressures are not intended to represent a precise measure of conditions near the substrate but instead illustrate an interesting trend. Both the Ta and C concentrations decline quickly as the N_2 partial pressure begins to increase followed by a slow decrease as N_2 partial pressure was further increased. In contrast, nitrogen concentration is very low without introducing N_2 flow and rises rapidly until saturated at a N_2 partial pressure of $\sim$1.5 mTorr. The nitrogen content in the films mainly comes from TBTDET precursor decomposition, the incorporation of N by Ta species that are sputtered from the target, and molecular TaN sputtered from the target. The chemical component is taken as constant in the model because nitrogen species are not included as enhancing agents of the chemical reactions. Therefore the nitrogen concentration saturates at a lower N_2 partial pressure than the experimental results.

Although the precursor concentration in the chamber is regarded as unchanged for this group of experiment since the carrier gas flow rate and the precursor vapor pressure are not varied, the nitrogen content in the films is not the same. This is due to the nitrogen plasma acting as a reducing agent in the chemical reactions as well as the reactive gas in the reactive sputtering process. According to AES, the nitrogen concentration without N_2 introduced into the chamber (0 mTorr in Fig. 6) is as low as 5%, suggesting that the precursor dissociation into TaN is difficult without the nitrogen plasma. Most likely the nitrogen atoms in TBTDET are prone to join the volatile organic by-product and leave the substrate surface at zero N_2 flow rate. The modeling results support this conjecture. The film nitrogen concentration first increases linearly with N_2 partial pressure and then becomes saturated as the N_2 partial pressure increases beyond 1.8 mTorr. The saturation should be caused by the limitation of the Ta source to the substrate. The target is found to be heavily covered by tantalum nitride at 2.4 mTorr. It is then in "poison mode." In this event, Ta sputtering is suppressed resulting in weaker ion bombardment to the substrate surface than in metallic mode, explaining the relatively high oxygen contamination (7%). The Ta and C concentrations decrease with the increase of N_2 partial pressure, as shown both by the experimental points and by the simulation curves.

Modeling results of the target coverage by the three components show (in Fig. 7) that target coverage by nitride increases with the N_2 partial pressure, while the coverage by hydrocarbons is negligible. In the experiments, the target presented a nitride color at a N_2 partial pressure of 1.8 mTorr. This is consistent with the simulation prediction if we use the criteria that 60% TaN coverage means poison mode in the model.

2. *Effect of sputtering gas* (Ar)

Ar is introduced to the chamber through both the carrier gas line and the bypass line. If the carrier gas flow rate is fixed, a high flow rate of bypass line Ar can increase the sputtering of the Ta target and result in a high flux of Ta and Ta^+ ions being delivered to the substrate region. (Elevating the target power has a similar result.) Gas phase momentum transfer resulting from the same ion bombardment may also serve to inhibit the diffusion of volatile organic products away from the sample surface. On the one hand, confinement of volatile organic species near the surface would help prevent contamination of the target and the upper process cham-

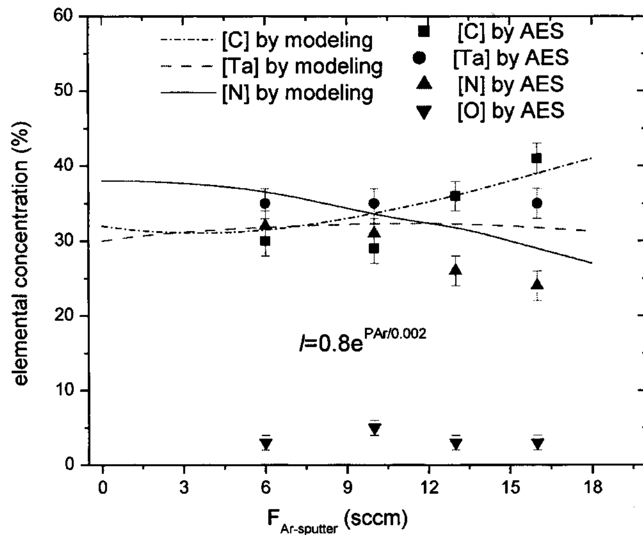

FIG. 9. Comparison of experimental results and modeling calculation of film composition variation vs Ar sputter gas flow rate after the definition of l is corrected. Other working conditions are listed in Table I. l is an exponential function of $F_{\mathrm{Ar\ sputter}}$.

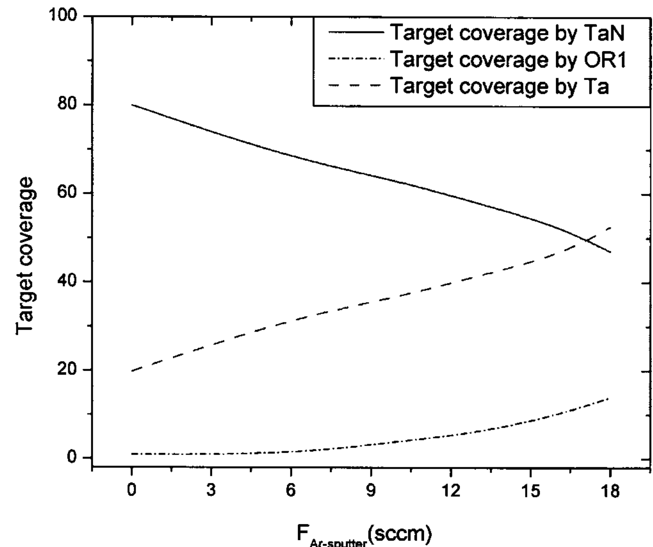

FIG. 10. Modeling results of target coverage variation vs Ar sputter gas flow rate.

ber. On the other hand, confinement may increase the organic content in the film. The AES analysis of the resulting films (shown in Fig. 8) does not detect changes in Ta concentration, but carbon concentration increases from 29% to 41% and nitrogen decreases from 32% to 24%. The model does not successfully predict these trends, though the absolute magnitudes are well represented. This indicates that some physics are either missing or poorly simulated.

The discrepancy may be due to neglecting the mechanism of elastic scattering when considering the confinement region. Therefore the results of the film composition shown in Fig. 8 only reflect the enhanced sputtering and deposition of the Ta and TaN. Although we hypothesize that the ion bombardment inhibits the diffusion of OR2 by means of elastic momentum transfer and promoting the conversion from OR2 to OR1 in the substrate region, we do not use the latter mechanism in the model. We can simulate the effect by choosing to formulate the stoichiometry number l of OR1 in reaction (4) as an exponential function of the Ar partial pressure, meaning that the generation rate of nonvolatile organic molecules (OR1) increases with the ion bombardment nonlinearly while the volatile organic molecules (OR2) remain constant. For example, increased Ar ion bombardment breaks up CH_4 on a surface into C's and H's which stick. Clearly then l is dependent on ion bombardment and increases with Ar. The Ar partial pressure consists of both the bypass line Ar flow and the carrier gas flow. Instead of using l equal to 3, at Ar partial pressure of 0.0028 Torr, let l vary as

$$l = 0.8e^{P_{\mathrm{Ar}}/0.002}$$

and m remain fixed at $m=2.02$.

Figure 9 shows that the correction in l significantly changes the simulated result of film composition in the way that carbon concentration increases with the Ar sputter gas flow while nitrogen decreases. Ta concentration is barely affected by the Ar sputter gas as seen in the experiments. Therefore by comparing this model to the experiments, the elastic scattering mechanism is identified as an important process.

The simulation results of target coverage (in Fig. 10) show that nitride coverage decreases with the Ar sputter gas due to increased number of target sputtering events. More Ta sites are exposed accordingly. The gradual incline of OR1 coverage on the target indicates that the higher flux of OR2 results from the increased Ar sputter gas. This is caused by the increased OR1 generation rate resulting from the specific definition of l as discussed above. Under the experimental conditions, the target remains metallic at Ar flows above

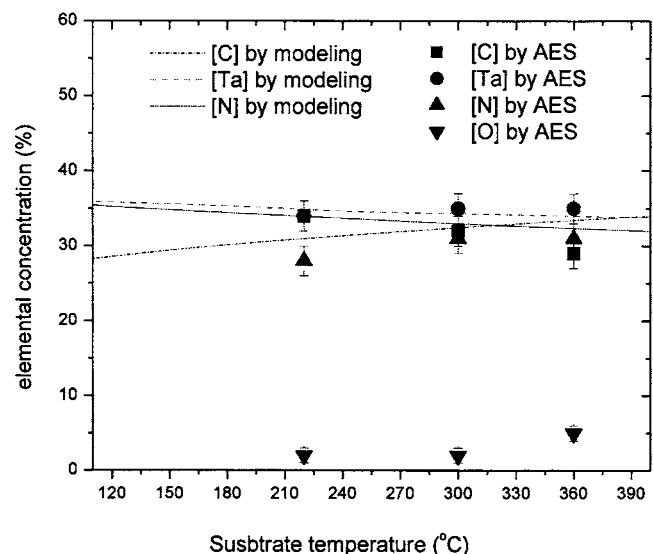

FIG. 11. Comparison of experimental and simulation results for substrate temperature effect on elemental composition. Other working conditions are listed in Table I.

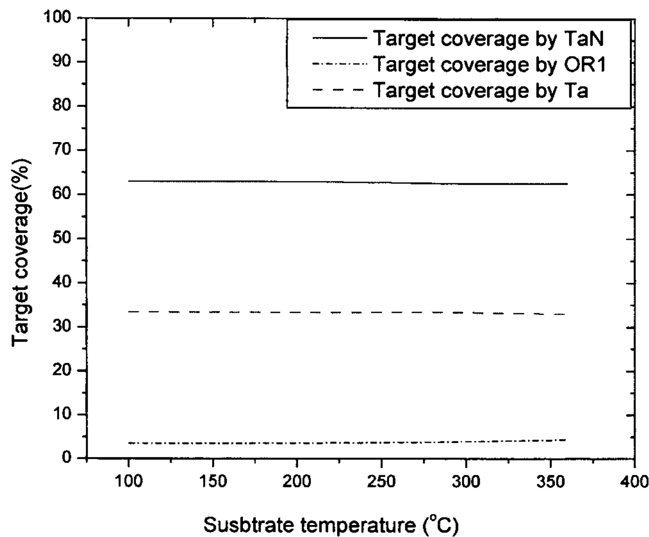

FIG. 12. Modeling result of target coverage vs substrate temperature. Other working conditions are listed in Table I.

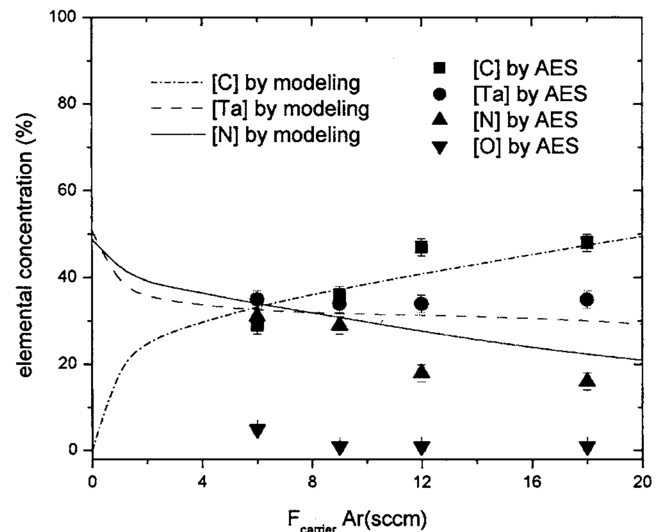

FIG. 13. Comparison of the experimental and modeling results of elemental compositions vs Ar carrier gas flow rate. Other working conditions are listed in Table I.

~5 SCCM. The model results also show that both nitride and OR1 coverage are below 60% at approximately the same flow rates.

Owing to the modification of l, the OR1 and OR2 creation rate and flux increase with Ar flow rate. Both the substrate surface and the target surface are occupied with more OR1 sites (Figs. 9 and 10). Nitrogen sources are regarded as unaffected by the Ar flow rate change.

3. Effect of substrate temperature

One of the anticipated advantages of the CEPVD process is that ion bombardment increases surface energy and decreases the demand for high substrate temperature, while making low resistivity films.[18] To check this, the substrate temperature is varied from 350 °C down to 250 °C in the CEPVD experiments. The elemental composition from both AES and the modeling is compared in Fig. 11.

In CEPVD, plasma generated particles convey significant energy to encourage the chemical reactions through the plasma sheath acceleration, in the range of several eV to tens of eV. Substrate heating, in the magnitude of 0.1 eV, is no longer the major source of energy to activate the chemical reactions as in conventional CVD. Both the experiment and model show that changing the substrate temperature from 200 to 360 °C does not significantly change the film composition or the target coverage (Fig. 12).

Among all the concerned reaction rate coefficients, only k_4 is treated as a function of substrate temperature, namely,

$$k_4(\mathrm{m^3/s}) = 50e^{(T_{\mathrm{sub}}(^\circ\mathrm{C})-360)/60}. \tag{51}$$

As a result, the OR2 generation rate increases with substrate temperature. The TBTDET molecules may break up into more volatile molecules under higher temperature initially, but the plasma can effectively convert them immediately into nonvolatile molecules that deposit on the substrate. In other words, the confinement effect is more significant in determining the film composition than the temperature effect. Consistent with the experiments, the model shows that temperature causes a minor increase in carbon concentration at higher temperature due to the increase of the OR1 thermal velocity. The plasma parameters are assumed to be unaffected by the substrate temperature and the calculated values are listed in Table I.

4. Effect of carrier gas (Ar)

Ar carrier gas flow rate controls the delivery rate of the TBTDET molecules and also influences the plasma properties. Electron temperature drops while electron and ion densities increase with Ar flow rate. Increased TBTDET density results in a faster-than-linear increase of OR1 and OR2

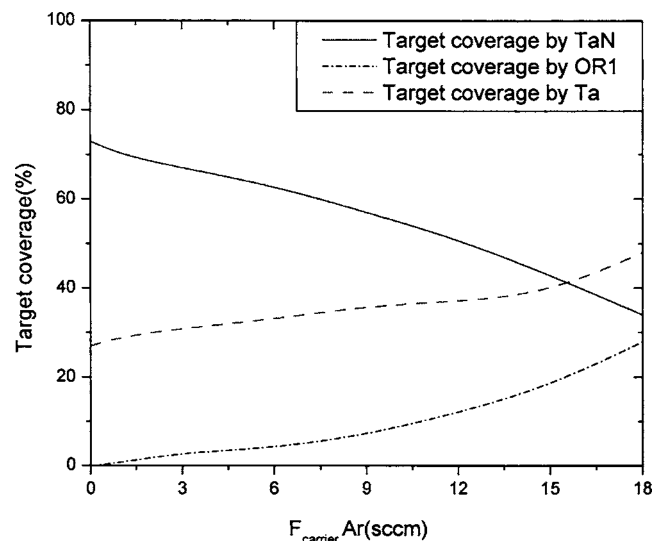

FIG. 14. Modeling result of target coverage at various Ar carrier gas flow rate. Other working conditions are listed in Table I.

fluxes. This is because the stoichiometry number l is related to ion bombardment in an exponential expression.

Employing the same values and expressions of the unknown factors determined through the previous discussion, the simulation results match the AES results of the elemental concentration very well (Fig. 13). Carbon concentration increases at higher carrier flow rate, while nitrogen decreases. Tantalum remains relatively constant.

Even though the Ar flow contributes to the target sputtering process, this mechanism is not considered in the model since no obvious change of target current is observed in the experiment and the current is input as a constant in the model. This means that Ar ion flux to the target is regarded as constant at varied Ar carrier gas flow rate. Therefore, the simulated OR1 and TaN coverages on the target (Fig. 14) may be higher than that seen in the experiment, where the metallic mode always results from this group of parameters.

The target coverage by OR1 increases abruptly with Ar carrier gas flow since the OR2 flux to the target becomes very high. The increasing rate of target sputtering is not as high as the OR1 formation rate on the target in the concerned range of Ar carrier flow rate.

IV. CONCLUSIONS

A semiempirical physical model has been developed to simulate the steady state CEPVD process by deriving the relationships between the back-end-processing parameters and the film atomic concentrations. Inductively coupled plasma (ICP) parameters were calculated based on a global analytical model. Based on the understanding of the experiment observations, the plasma-precursor-surface interaction was simulated by treating the electrons, ions, and hydrogen atoms as enhancing agents in the chemical reaction models. With a lump-sum assumption, the complex plasma chemistry environment was simplified such that all the organic byproducts are represented as either volatile (OR2) or nonvolatile (OR1) molecules. A number of unknown factors brought by the linear or nonlinear mathematical treatment of the undocumented physical relationships must be determined empirically to characterize the performance of a given CEPVD system. The model is then capable of predicting the variation trend of the film composition with the process parameters and the simulation results deviate from the AES results by less than 10%. The model guided the search for better process conditions and may guide equipment construction for advanced applications.

ACKNOWLEDGMENTS

The authors would like to acknowledge the Semiconductor Research Corporation (SRC Task ID 1035.01) and Novellus Systems for providing customized SRC funding for this research. Dr. Ron Powell from Novellus also provided valuable collaboration and insight. AES, XRD, XPS, and SEM were carried out in the Center for Microanalysis of Materials, University of Illinois, which is partially supported by the U.S. Department of Energy under Grant No. DEFG02-91-ER45439. The authors also wish to thank the undergraduate helpers, Crystal Manohar, Hussain Nomanbhai, and Ying Wu, for experimental efforts and data analysis.

[1]N. Li, D. N. Ruzic, and R. A. Powell, J. Vac. Sci. Technol. B **22**, 2734 (2004).
[2]P. Carisson, C. Nender, H. Barankova, and S. Berg, J. Vac. Sci. Technol. A **11**, 1534 (1993).
[3]S. Berg, H. O. Blom, M. Moradi, C. Nender, and T. Larsson, J. Vac. Sci. Technol. A **7**, 1225 (1989).
[4]L. B. Jonsson, T. Nyberg, and S. Berg, J. Vac. Sci. Technol. A **18**, 503 (1999).
[5]M. Moradi, C. Nender, S. Berg, and H.-O. Blom, J. Vac. Sci. Technol. A **9**, 619 (1990).
[6]H. Sekiguchi, T. Murakami, and A. Kanzawa, J. Vac. Sci. Technol. A **14**, 2231 (1996).
[7]M. FrenkLach and H. Wang, Phys. Rev. B **43**, 1520 (1991).
[8]J. Roth, in *Sputtering by Particle Bombardment II*, Topics in Applied Physics Vol. 52, edited by R. Behrish (Springer, New York, 1983), p. 91.
[9]W. Jacob, C. Hopf, and M. Schlüter, Appl. Phys. Lett. **88**, 204103 (2005).
[10]R. Zorat and D. Vender, J. Phys. D **33**, 1728 (2000).
[11]M. A. Leiberman and A. J. Lichtenberg, 1994, p. 73.
[12]M. A. Leiberman and A. J. Lichtenberg, 1994, p. 522.
[13]M. A. Leiberman and R. A. Gottscho, in *Physics of Thin Films*, edited by M. Francombe and J. Vossen (Academic, New York, 1994), pp. 1–119.
[14]J. C. Vickerman, *ToF-SIMS Surface Analysis By Mass Spectrometry*, edited by J. C. Vickerman and D. Briggs (IM Publications, Chichester/Surface Spectra, Manchester, 2001), p. 389.
[15]R. K. Janev, W. D. Langer, K. Evans, Jr., and D. E. Post, Jr., *Elementary Processes in Hydrogen-Helium Plasmas, Cross Sections and Reaction Rate Coefficients: Atoms+Plasmas*, edited by G. Ecker, P. Lambropouluo, and H. Walther (Springer, Berlin, 1987), Vol. 4, pp. 18–68.
[16]J. Hopwood, Phys. Plasmas **5**, 1624 (1997).
[17]D. R. Juliano, Ph.D. thesis, Modeling and measurements of an ionized physical vapordeposition device plasma, in Physics. University of Illinois, Urbana-Champaign, 2000, pp. 136–150.
[18]E. R. Engbrecht, Y.-M. Sun, S. Smith, K. Pfiefer, J. Bennett, J. M. White, and J. G. Ekerdt, Thin Solid Films **418**, 145 (2002).
[19]N. Matsunami *et al.*, At. Data Nucl. Data Tables **31**, 1 (1984).
[20]D. Zhang and J. K. Schaeffer, J. Vac. Sci. Technol. A **22**, 264 (2004).